Journal Name

ARTICLE

Imparting Gas Selective and Pressure Dependent Porosity into a Non-Porous Solid via Coordination Flexibility

Received 00th January 20xx,
Accepted 00th January 20xx

DOI: 10.1039/x0xx00000x

www.rsc.org/

Shyamapada Nandi,[ac] Phil De Luna,[c] Rahul Maity,[a] Debanjan Chakraborty,[a] Thomas Daff,[c] Thomas Burns,[c] Tom K. Woo,[c*] Ramanathan Vaidhyanathan[ab*]

Using a simple hard-soft acid-base concept we have deliberately designed gas-specific and pressure dependent porosity into a non-porous solid via coordination flexibility. This creates distinct gate-openings wherein the CO_2 molecule opens-up the framework pores by rotating the ligand about the weaker hard-soft bonds (Hard-Soft Gate Control). For this, we have studied the CO_2 gating behaviour of M(4-PyC)$_2$, (M = Mg, Mn and Cu), which represent metals of varying hardness. A combination of quantum chemical calculations, molecular dynamics and Grand canonical Monte Carlo simulations were performed to examine the gate opening of the isonicotinate ligands in Mg(4-PyC)$_2$. The simulations show that interaction of the CO_2 molecules with the isonicotinate ligands at different CO_2 loadings can result in pressure-dependent gate opening. Further, the simulated CO_2 uptake values calculated using the partially gate-opened structures at different loadings showed good agreement with the experimental uptake values. This provides an effective strategy for designing highly-stable dynamic porous solids employing rigid frameworks.

Introduction

Solids with metal-organic links provide a robust platform to carefully tune the properties at the metal site as well as offers access to improved pore space and chemistry by functional tuning of the organic ligands.[1-3] Though, stability and rigidity in a framework go in concert, a reversible dynamic character can be imparted to frameworks either via flexible organic linkers or localized ligand rotations- "gating" or through a structural transitions involving abrupt expansion/compression of the unit cell, induced by atomic displacement caused by interactive guest molecules- "breathing".[4] The flexibility of organic linkers has rendered some metal organic frameworks as soft porous materials.[3-18] Such dynamic frameworks in an extended solid has clearly been placed as an advantageous feature for guest encapsulation,[11-13,19-27] storage,[14,28,29] sensing[30-31] and biomedical application.[32-34]

Molecular-rotating gate[4] is a type of gating wherein rotation of the aryl rings is observed; only a limited number of such examples exist. Kitagawa and co-workers[35] reported a layered-pillared structure where the aryl ring could rotate as a function of hydration. Unfortunately, in this particular case, the dehydration and the concurrent gate opening resulted in a decrease of porosity. More recently, Schroder and co-workers found that the pyridyl rings in their linkers rotate in the presence of CO_2 to open the channels based on molecular simulations, powder XRD (PXRD), and IR experiments.[24]

Alternatively, the MOFs can 'breathe' upon gas adsorption, for example, in MIL-53(Sc) (Materials of Institut Lavoisier, L^{2-}= 1,4-benzenedicarboxylate (BDC)) the flipping of the carboxylate bonds of the BDC units causes breathing. Interestingly, this happens only at elevated temperatures making it a thermo-mechanical process.[36] With this framework breathing large structural changes are observed in the X-ray and neutron diffractions. The breathing in this metal (hydroxy) carboxylate framework of MIL-53 is due to the strong CO_2 interactions with corner-sharing μ_2-OH groups, which has significant electrostatic component to it.[37] In contrast, the oxo anion based clusters do not seem to favour the CO_2 assisted breathing.[38-43]A thorough examination of the literature reveals that the μ_2 or μ_4-oxo anions are much more ubiquitous in the SBUs of MOFs compared to the bridging hydroxyl groups. These statistics suggest that building a library of dynamic frameworks by incorporating 'hydroxyl' moieties capable of interacting strongly with CO_2 is not straightforward. Aforesaid calls for developing CO_2 interactive functionalities that are more easy to plug-in into a MOF framework to gain CO_2-specific dynamicity via either gating or breathing.

In most cases, the breathing behavior is triggered by solvents,[9,12,14,15,26,36,44-46] whereas there are only a few cases where a gas alone is able to trigger the breathing.[19,13,25,47,48] With the exception of one material,[24] all these breathing behaviors under a purist's argument are associated with significant lattice changes as compared to a gate-opening

[a] Department of Chemistry, Indian Institute of Science Education and Research, Pune, India.
[b] Centre for Energy, Indian Institute of Science Education and Research, Pune, India.
[c] Centre for Catalysis Research and Innovation, Department of Chemistry, University of Ottawa, Canada.
† Footnotes relating to the title and/or authors should appear here.
Electronic Supplementary Information (ESI) available: [PXRD, TGA, IR, Adsorption studies, Computational details]. See DOI: 10.1039/x0xx00000x

assisted by localized bond rotations. Moreover, the gating in the materials have all have made a moderately porous framework into a more open or less porous framework.[13,14,19-28] In many cases, there is no significant change in the pore volume but a marked impact is seen in the adsorption capacity.[49-52] None have completely closed off the adsorption of the guests, let alone do so selectively. Such gating has been observed in both low and high pressure adsorption. This pressure-controlled change in porosity makes these materials operate like a switch to detect specific gases present above or below certain partial pressures. When they occur at larger pressures, the very phenomenon could provide stimuli-responsive smart separation membranes.

Generally, the interactions of gases with organic or metal-organic frameworks are of the order of 4.8 to 12 kcal/mol, which is lower in comparison to those exhibited by solvents, for example, water (10.8-15.5 kcal/mol). However, gas-adsorbent interactions can co-operatively possess sufficient energy, even at extremely low partial pressures, to cause significant modifications on the structure by manipulating specific sites of the ligand.[4,6,19,25,26,37,53-54] In this study, we constructed three ultra-microporous MOFs using metals with systematically varying hardness (Hardness order: Mg > Mn > Cu). These MOFs are Mg(4-PyC)$_2$ (**1**, IISERP-MOF21a), Mn(4-PyC)$_2$ (**2**, IISERP-MOF21b), and Cu(4-PyC)$_2$ (**3**, IISERP-MOF21c) (where 4-PyC = 4-pyridylcarboxylate or isonicotinate). The first two of which exhibit pressure dependent, CO_2 specific gate opening. Importantly, **1** and **2** are non-porous and do not adsorb gases except in the presence of CO_2, which triggers a gate opening. With **1**, the gate opening occurs at a low partial pressure of CO_2. We have exploited the concept of hard-soft acid-base (HSAB) theory by utilizing the metal as a hard Lewis acid and the organic ligand serving as a borderline hard base to aptly tune their coordination strengths- Hard-Soft Gate Control (HSGC). This introduces coordination flexibility assisted gate-opening that converts an otherwise non-porous material into an ultra-microporous material with nominal surface area (~350-400 m^2/g). The CO_2 adsorption data suggests there are two gate opening events that occur with minimal changes in the crystal lattice of the material. Atomistic modelling reveals how CO_2 interactions with the organic linkers can provide sufficient energy to induce the bond rotations responsible for the gate opening events. Since the molecular-rotation assisted gating in **1** is not accompanied by any marked structural change(s) it becomes difficult to snapshot the open/closed structures corresponding to the pre- and post-gate opened phases from experiments. We have gathered these insightful snapshots from computational modelling.

Results and Discussions

Materials were synthesized via a solvothermal reaction between M(acetate)$_2$ (M= Mg/Mn/Cu) and 4-pyridine carboxylic acid (4-PyC) in a DMF/Acetonitrile or DMF/EtOH/THF mixture by heating at 110-120°C for 72hrs (Supp Info). The Mg(4-PyC)$_2$, **1** and Mn(4-PyC)$_2$, **2** were scaled up to 10 g in laboratory synthesis. **1** and **2** are isostructural whereas Cu(4-PyC)$_2$, **3** is slightly different from the other two. Hence, we are explaining the structure of **1** as a representative. **1** has a cubic three-dimensional framework built up from the linking of Mg centers by 4-PyC aka isonicotinate (Figure 1). There are two crystallographically unique Mg centers which are connected by the μ_2 bridging carboxylate units to form chains. The Mg(1) and Mg(2) alternate within the chain. Importantly, the chains are made up of Mg^{2+} octahedra wherein the carboxylate oxygens occupy the equatorial positions and the pyridyl nitrogens occupy the axial positions (Figure S1A). Four such chains running along the a-axis are positioned in the bc-plane in a square lattice disposition. The alternate chains are rotated by 90° with respect to each other (Figure 1B). The linking of these chains in all three crystallographic directions by the 4-PyC units results in the 3-D cubic framework. Also, in **1** and **2**, the alternate 4-PyC rings are rotated by ~90° with respect to each other which generates an ultra-microporous 1-D channel along the a-axis (5.5 x 6.5 Å, not factoring the van der Waal radii, Figure 1A and S1). The c- and b-axes do not contain any pores or channels. These 1-D channels are occupied by DMF guest molecules. Notably, in **3**, the aromatic rings of the 4-PyC units are not rotated with respect to each other, leading to a larger channel (8.6 x 8.8 Å. Figure S3).

Considering the presence of just an ultra-microporous 1-D channel (Figure 1A), we expected this material to be non-porous or to have negligible porosity. Accordingly, the 77 K and 298 K N_2 adsorption showed no gas uptake; however, the 195 K and 298 K CO_2 adsorption showed saturation uptakes of

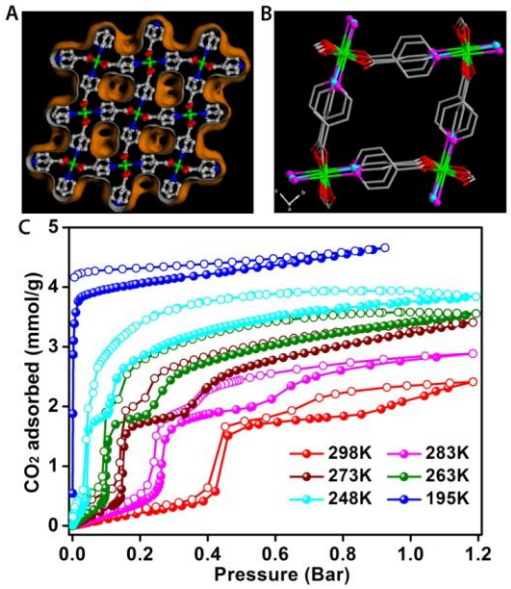

Figure 1. (A) Experimentally determined single crystal structure of Mg(4-PyC)$_2$, **1**, with its Connolly surface represented. The Mg centers are linked by 4-PyC units that form a cubic three-dimensional lattice. Color scheme: Green-Mg; Grey-C; Blue-N; Red-O. Hydrogens are omitted for clarity. (B) A single channel has been shown, and the pyridyl nitrogens have been color coded to indicate the presence of two different Mg-N distances within the lattice. The purple ones have Mg(1)-N distance = 2.22 Å, and the cyan ones have the Mg(2)-N bond distance = 2.20 Å. Both Mg(1) and Mg(2) bind to carboxylate oxygens strongly (av. Mg-O distance = 2.05 Å). (C) Adsorption-desorption isotherms (closed and open symbols, respectively) of 1 for CO_2 collected at different temperatures.

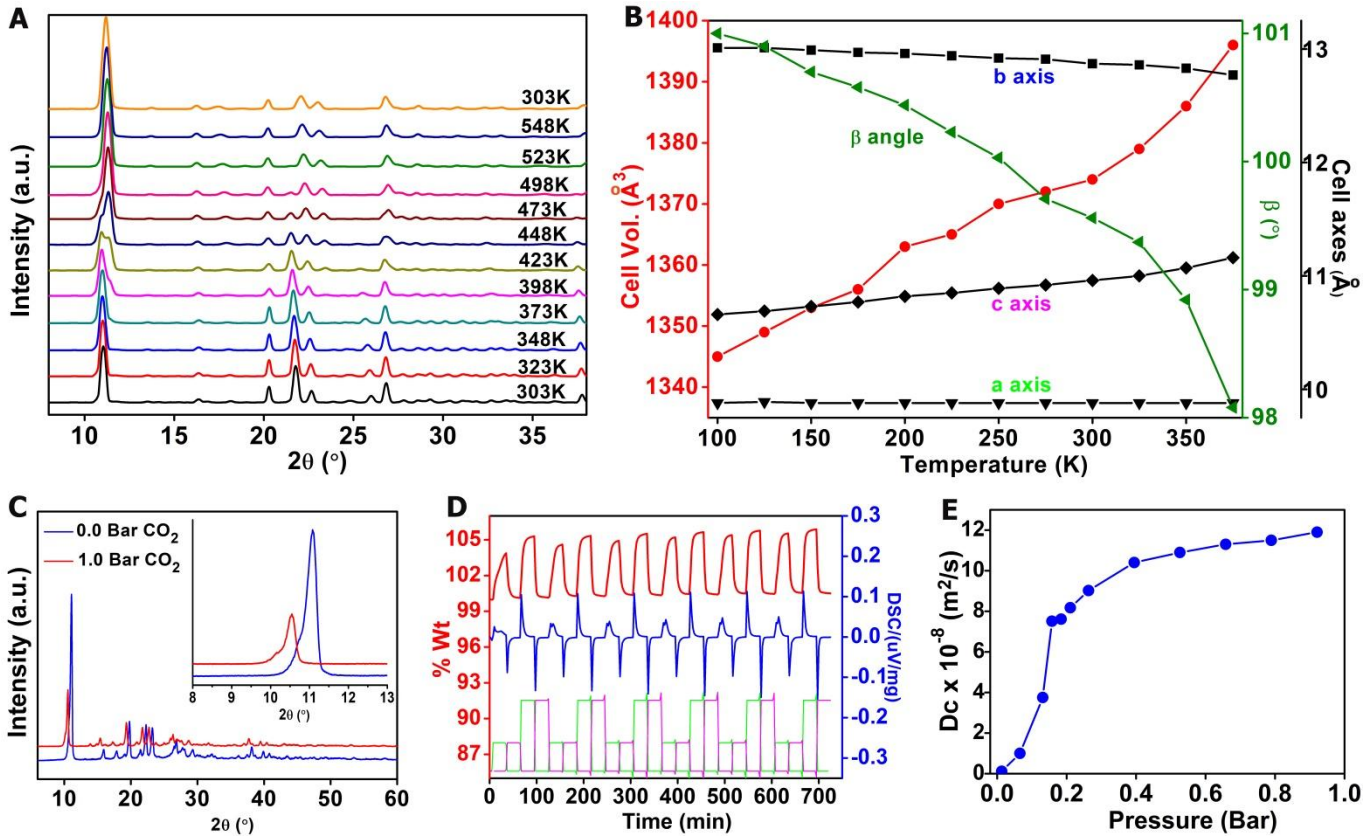

Figure 2. (A) Variable temperature PXRD plots of the as-synthesized form of **1**. The plots at 303 K (orange) shows the stability of sample heated at 548 K and cooled back to 303 K. (B) A plot of the change in single crystal unit cell parameters of **1**, obtained from single crystal diffraction, as a function of temperature. (C) A comparative PXRD study of activated and CO_2 loaded sample (under an environmental cell). The peak due to (011) reflection shifts to lower 2θ values when the sample was maintained at 1 bar of CO_2. This suggests expansions along the b and c- directions upon CO_2 sorption. (D) TGA cycling of **1**, with alternating flows of CO_2 and N_2. The cycle involves N_2-20 ml, CO_2-20 ml, N_2-50 ml, CO_2-50 ml, N_2-20 ml, CO_2. (E) Plot of the self-diffusion coefficient of CO_2 in **1** as a function of CO_2 pressure.

4.7 mmol/g and 2.42 mmol/g, respectively. In this ultra-microporous framework of **1**, built from short linkers, CO_2 gas is capable of generating a stepped isotherm showing an abrupt increase in pore accesses (Figure 1C). This increase in CO_2 uptake occurs at two different pressure points and is observed only for CO_2. In **1**, at 273 K, there is no significant porosity prior to the abrupt increase in CO_2 uptake at 0.1 bars. What we observe in **1**, is a gating phenomenon.[4,25,36] With this interpretation, at 273 K, with a CO_2 pressure of 0.1 bar the uptake jumps-up from 0.3 mmol/g to 1.7 mmol/g, indicating the first gate opening (Figure 1C). Thus, with a pressure differential of just 0.1 bar, the uptake sharply increases (~82%) suggesting the fast switching even in these rigid MOF. As the CO_2 pressure is further increased to 0.3 bar again the uptake abruptly jumps-up from 1.8 mmol/g to 2.6 mmol/g, indicating second gate opening (Figure 1C). The gate opening is persistent across different temperatures (298, 283, 273, 263 and 248 K), however, the pressure at which both gate openings occur moves to lower values as the temperature decreases. Additionally, the pressure difference between the two gate opening points becomes smaller as the temperature decreases. At 195 K the trend suggests that the gate is already fully opened at very low pressures.

To ascertain if these gate openings are assisted by any temperature effects, variable temperature PXRD measurements were carried out in the temperature range of 303 to 548 K under 10^{-3} vacuum as shown in Figure 2A. The PXRD plots indicated the lack of any major structural changes. The (011) peak does shift from 2θ of 11.0 to 11.35° as the temperature reaches ~445 K indicating a slight structural contraction likely due to loss of DMF. The same peak then shifts back to lower angles as the temperature is raised beyond 445 K, likely due to lattice expansion. Above this temperature, the crystallinity remains intact even until 548 K. This is in agreement with the exceptional thermal stability (up to 450° C) observed from the TGA (Figure S11 and S12). Such high thermal stability is quite unusual and, to the best of our knowledge, unreported for an Mg-pyridyl based compound. Furthermore, we have carried out variable temperature single crystal X-ray diffraction studies. Figure 2B gives a plot of the unit cell parameters as a function of the temperature determined from single crystal diffraction study. The plot

reveals that the b- and c-axes showed subtle changes, while a-axis showed no change as the temperature is varied from 100 K to 375 K. Within the same temperature range, the monoclinic beta angle only decreases from 101 to 98°. These small changes in the unit cell parameters point to only minor structural changes, possibly due to solvent loss. This suggests the gate opening is not due to a major structural change. On the other hand, linker rotation as the mechanism of gate opening is consistent with this data since it should not change the cell parameters significantly.

The bond distance analysis from the single crystal structure shows the carboxylate groups forming rigid bonds with the Mg (average Mg-O = 2.05 Å), while the pyridyl nitrogens form relatively weaker bonds based on typical Mg-O and Mg-N bond lengths. There are two types of Mg-pyridyl bonds – one with a Mg-N bond length of 2.20 Å (Mg(1)-N) and the other with an 2.22 Å (Mg(2)-N) bond length. The rotation of the pyridyl ring along Mg-N bond is likely to be responsible for the gate opening.

The gate opening behaviour was further characterized via in situ PXRD measurements under CO_2 environment (using an environmental cell). Figure 2C shows the comparative PXRD plot of activated vs. CO_2 (1.0 bar) loaded sample. The peak due to 011 reflection shifts (2θ =11-10.5°) to lower 2θ value upon loading with 1 bar CO_2. This indicates the subtle expansion of the lattice during the gate opening.

A TGA cycling experiment was carried out using **1**, where the CO_2 flow rate was set to low (20 ml/min) and high (50 ml/min) values. It could be seen that there was a quantitative difference between the CO_2 uptakes when the CO_2 flow was varied between cycles (Figure 2D). Each CO_2 cycle included a 20 ml CO_2 flow, followed by a 20 ml N_2 sweep and then by a 50 ml CO_2 flow which is swept with a 50 ml N_2 flow. A comparison of the DSC trace between the 20 ml and 50 ml CO_2 flow cycles shows the possibility of CO_2 accessing different sites at different flow rates. Considering that the 20 ml and 50 ml flows mimic the low and high pressure CO_2 adsorption equilibrium points, it is possible that there are distinct sites. Under 50 ml/min flow all the sites fill up immediately where as in case of 20 ml/min flow the distinct sites fill up gradually.[55] For the 20 ml flow, there are two exothermic DSC peaks as compared to just one for the 50 ml flow. This could suggest the sites accessed during the different flows are different. Of course, there does exist an alternate interpretation involving the slow equilibration of the CO_2 uptake with the 20 ml flow compared to the 50 ml flow; however, it would not explain the presence of two DSC peaks in the lower flow cyclings nor its marked difference from the DSC profile observed for the 50 ml cycle. Also, a routine CO_2 on-off cycling on a TGA at a constant flow of (either 20 ml or 50 ml) con-firmed facile adsorption-desorption of CO_2 (Figure S15 and S16).

1 lies in the borderline of being non-porous or porous. Thus, any small structural change could produce a significant change in the accessibility of the porous spaces within the material and the associated CO_2 kinetics. This can be tracked from the changes in the CO_2 self-diffusion coefficients during the gate-opening processes. For this purpose, we carried out a rate of adsorption experiment at 273 K in the pressure range of 0-1 bar and 8 different pressure points were used to determine the diffusion coefficients by fitting them against a slit/spherical pore models (Supp info). Interestingly, the self-diffusion coefficient showed an appreciable jump (9.9×10^{-9} to 6.5×10^{-8} m^2/s) at the low pressure gate opening point (0.1 bar) and a relatively lower jump(7.5×10^{-8} to 9.1×10^{-8} m^2/s) at the higher pressure gate opening (0.3 bar) (Figure 2E). Above this pressure, the diffusion steadily increases to a value of 12×10^{-8} m^2/s giving almost two orders of magnitude increase in diffusion as we progress from the lowest partial pressure to 1 bar. This is quite high compared to diffusion in zeolites and some of the other metal organic frameworks.[56-59]

The gate opening happens at a CO_2 pressure of 0.1 bar at 273 K giving a CO_2 uptake of 1.7 mmol/g (82% increase w.r.t the unopened form). When the CO_2 pressure is 0.3 bar, the total uptake reaches the highest capacity of 3.4 mmol/g (~31% increase w.r.t. the partially opened form at 0.1 bar pressure). The gate opening pressure shifts to lower pressures as we go down in temperature, where at 195 K, a condition that mimics high pressure adsorption, the gate is fully open with a maximum saturation capacity of 4.7 mmol/g is observed (Figure 1C). A Non-localized Density Functional Theory (NLDFT) model of the 195 K isotherm shows the presence of uniform 3.95 Å pores (Figure S24). The surface area turns out to be 357 m^2/g for 1. Due to the complex gate opening, the 273 K CO_2 isotherm could not satisfactorily be modelled using NLDFT (Figures S26 and S27).

A striking aspect of the gate opening in **1** is that only CO_2 is capable of inducing conformational changes and neither $N_2/CH_4/O_2/15CO_2{:}85N_2$ nor heat is able to impart any structural flexibility. To understand this selectivity and examine the energetics of the ligand rotation to substantiate our above multiple site gate opening model and we studied the process with a combination of DFT calculations, grand canonical Monte Carlo (GCMC) simulations and molecular dynamics (For computation details see the supporting information). We focus on the CO_2 adsorption isotherm at 273 K because at this temperature the uptake has two clearly defined steps in the uptake – one at about 0.15 bar and one at about 0.38 bar (Figure 1C). If a gate opening phenomenon were responsible for the step changes in the CO_2 uptake, there may be additional conformations of **1** that have more open or more closed pores. As noted earlier, **1** has two distinct Mg-N bonds. Looking down the 1D channel, as shown in Figures 1B and S1, it can be seen that the pyridyl rings with the different Mg-N bonds are roughly perpendicular to one another. By rotating these pyridyl rings, one can further open or close the channels. Using periodic DFT calculations, we performed an exhaustive search where various combinations of the pyridyl rings were rotated to varying degrees to widen or close the channels. Starting from 18 different initial structures (See supporting information, Figure S34), only 5 thermodynamically stable structures were identified, including one that corresponds to the crystal structure (Figure 3A). These structures are labelled conformers **1a-d** and are shown in

Figure 3A starting at the left with a fully closed structure moving to more open pore structures towards the right. The DFT calculated energies relative to the crystal structure conformation, **1c**, which had the lowest energy, are given below the structures.

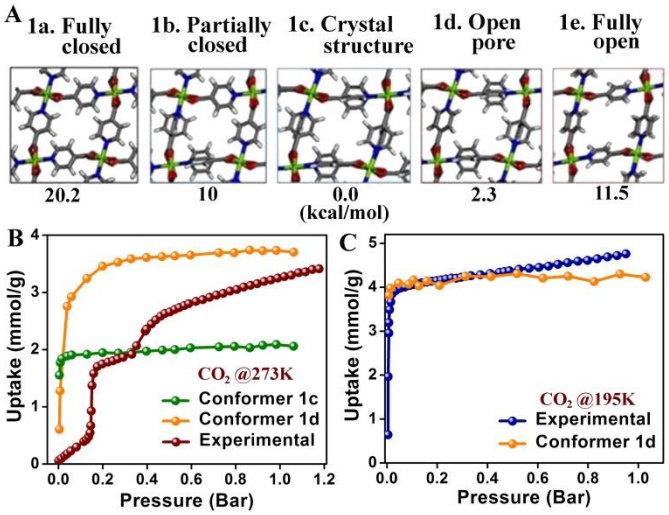

Figure 3. (A) Minimum energy DFT optimized conformers of 1. Energies reported are relative to conformer 1c. (B) Computed isotherms using the structure of 1c and 1d compared to the experimental isotherm at 273 K. (C) Comparison of the experimental isotherm to the simulated isotherm with conformer 1d at 195 K.

Using each of the DFT optimized structures shown in Figure 3, simulated CO_2 adsorption isotherms were calculated at 273 K. The 'fully closed' and 'partially closed' structures, **1a** and **b** did not show any CO_2 adsorption from the GCMC simulations showing that these conformers have no CO_2 accessible pore space. The conformer corresponding to the crystal structure, **1c**, has accessible pore space and its calculated adsorption isotherm (using the DFT optimized structure) shows that the CO_2 uptake rapidly reaches a saturation uptake of approximately 1.9 mmol/g (Figure 3B). This uptake is close to the uptake in the experimental isotherm at 273 K observed in the range 0.18 – 0.38 bar between the first and second gate opening 'events'. The experimental isotherm of **1** is also shown in Figure 3B for comparison. The next conformer, **1d**, has a saturation uptake at 273 K of approximately 3.5 mmol/g. This is also consistent with the maximum uptake observed in the experimental isotherm. Notably, this conformer is only 2.3 kcal/mol less stable than the crystal structure, and it is conceivable that interactions between the framework and CO_2 molecules may provide enough energy to access this structure. The final conformer located, **1e**, is a fully open structure that is 11.5 kcal/mol higher in energy than the crystal structure. A simulated isotherm (not shown) with this structure gave a saturation uptake of 5 mmol/g, which is significantly higher than the saturation uptake observed experimentally.

From the calculated isotherms and relative energies of the conformers, we hypothesized the crystal structure conformer, **1c**, gives rise to the uptake at the plateau (0.18 – 0.38 bar) after the first gate opening. Then as the pressure increases beyond 0.4 bar, we further hypothesize that conformer **1d** becomes more accessible giving rise to gradually higher CO_2 uptake as the pressure increases. In other words, conformer **1d** corresponds to the final 'gate opened' structure. The fully open structure, **1e**, is not likely to be accessible since it is too high in energy (+11.5 kcal/mol relative to **1c**) and since it's saturation uptake of 5 mmol/g is much higher than observed for **1** at any temperature. At this point, we have no evidence to suggest that the closed pore conformers **1a** or **b**, are responsible for the low uptake at the low pressure regime observed before the first gate opening. The primary reason for this is that these conformers are quite high in energy (+10.0 and 20.2 kcal/mol). Additionally, they show no CO_2 uptake, while experimentally there is a modest uptake of CO_2 in the low pressure region.

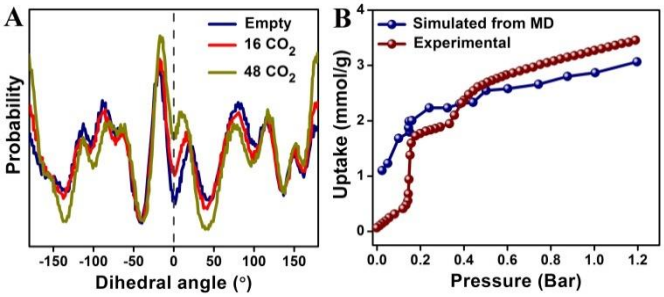

Figure 4. (A). Distribution of dihedral angles of the pyridyl rings from a 1 ns MD simulation of a 3 x 2 x 2 supercell of 1. 16 CO_2 per supercell corresponds to the uptake observed at a pressure of 0.15 bar while 48 CO_2 molecules corresponds to the uptake at a pressure of 1.25 bar. (B) Simulated isotherm where each pressure point is an average uptake calculated from 3 snap shots derived from MD simulations where the pyridyl ligands were free to rotate.

If structure **1d** corresponds to the final gate opened structure responsible for high pressure uptake, then the low temperature 195 K adsorption isotherm of **1d** would ideally match that of the experimental isotherm of **1** at 195 K because low temperature can be used to mimic high pressure. As shown in Figure 3C, the simulated isotherm of **1d** is in good agreement with the experimental isotherm at 195 K, which further supports our hypothesis.

To provide insight into the CO_2 pressure dependent conformational changes, we performed molecular dynamics simulations at 273 K at fixed CO_2 loadings. To do this more accurately, we fit the torsional potentials of a force field involved in the rotation of the pyridyl rings to a torsional scan calculated at the DFT level. The details of the fitting and validation are given in the Supporting Information. The fitted potential was in reasonable agreement with the DFT potential and reproduced the overall barrier to rotation of ~10 kcal/mol.

A series of 1 ns MD simulations were performed wherein the MOF framework was fixed except that the pyridyl rings were allowed to rotate with the approximate fitted potential. More specifically, simulations were performed on a 3 x 2 x 2 supercell of **1** at 273 K with a range of loading from zero to 44

CO_2 molecules per supercell. 44 CO_2 molecules correspond to the loading observed at a pressure of 1.2 bar.

First, we examined whether the presence of CO_2 molecules was able to change the conformation of the pyridyl rings. For this, we examine the distribution of pyridyl dihedral angles defined such that 0° and ±180° correspond to open pores and ±90° corresponds to closed pores. The distribution resulting from a MD simulation of **1**, with no CO_2 molecules, 16 CO_2 molecules and that containing 48 CO_2 molecules show significant differences in the pyridyl ring conformations as a function of CO_2 loading (Figure 4A). At the highest loading of 48 CO_2 molecules, there is a significant increase in the open pore con-figurations at 0° and ±180° as compared to the empty simulation. To quantify the change in dihedral angles, the ratio of open to closed dihedral angles was calculated. With zero loading or no CO_2 molecules, it was found that this ratio was 1.05, which corresponds to a 1:1 mixture of dihedral angles in open and closed positions. With 48 CO_2 molecules in the simulation cell, the number of pyridyl rings in the open position is double that in the closed position. Figure 4A also gives the dihedral distribution from an MD simulation with 16 CO_2 molecules revealing that it is intermediate between the distributions resulting from the empty and fully loaded MD simulations. Thus, the simulations suggest that CO_2 loading can induce large conformational changes of the framework's pyridyl rings to widen the pores.

To see how these conformational changes would allow for the differential CO_2 uptakes that were experimentally observed, we performed MD simulations with 16 different CO_2 loadings corresponding to pressures from 0.02 to 1.2 bar. Snapshots of the MOF framework were then taken at 0.6, 0.8 and 1.0 ns and used to calculate the adsorption uptake (using GCMC simulations) at each pressure by taking the average from the three snapshots. Shown in Figure 4B is the adsorption isotherm where each point was determined using snapshot geometries from the MD simulations. Although the average uptake was determined using geometries from only three snapshots, we note that the 3 x 2 x 2 simulation cell accounts for a large number of pyridyl rings. Calculated in this way, the greatest standard deviation in uptake was found to be only 0.21 mmol/g. Considering how simple our model is, the simulated isotherm shows good agreement with the experimental isotherm for pressures greater than ~0.1 bar, or from the first gate opening onwards. Neither of the abrupt changes in uptake observed at 0.2 bar and 0.4 bar is seen in the simulated isotherm. However, the gradual rise in the CO_2 uptake from 0.4 bar onwards is reasonably well reproduced. This suggests that a gradual gate opening induced by the guest CO_2 molecules can explain the adsorption in this region.

So far, the simulations have been able to provide a reasonable explanation for the experimental isotherm from 0.18 bar to 1.2 bar via a conformational change from crystal structure conformation, **1c**, to the open pore structure, **1d**. However, the initial low pressure regime with low CO_2 uptake is still unexplained. We could not identify a low energy conformer of **1** with closed pores. The two closed pore conformers identified were 10.0 and 20.2 kcal/mol higher in energy than the crystal structure and therefore would have negligible populations at the temperatures considered here. One observation from the MD simulations of the empty framework is that the linker rotation was rapid and dynamic without any CO_2 molecules. The Connolly surfaces (calculated with a probe radius of 1.72 Å which corresponds to CO_2) calculated on several snapshots from the MD simulation show that the channels are no longer connected because of the linker rotation. Thus, at any given time, the empty framework possesses many pyridyl rings in the 'closed' position, perpendicular to the channel that prevents CO_2 diffusion into the MOF, which may explain the low uptake at low pressure. Another possible explanation for the minimal uptake from 0 bar to 0.18 bar is that it is a surface effect. More specifically, at the surface of the crystals, the pyridyl rings may have a low energy conformation that somehow blocks off the entry of CO_2. Then it is possible that the surface pyridyl rings are opened at a certain CO_2 pressure, resulting in the first gate opening. Since surface reconstruction is often a long time and length scale process and potentially very complex, we have not performed any simulations to examine it.

The crux of the CO_2 adsorption in **1** lies in the choice of the framework components which brings dynamic behaviour to a rigid framework. The gate opening mechanism is facilitated by the co-ordination flexibility of the Mg-N bonds. Mg^{2+} is a hard Lewis acid, whereas the pyridyl is typically a borderline soft base. This mismatch provides sufficient coordination flexibility to allow for the gate opening which in turn produces a significant change in the accessibility of the ultra-microporous channels within the material. To evaluate the applicability of the Hard Soft Acid Base (HSAB) principle to provide coordination-assisted rotational flexibility, we attempted to synthesize the isostructural analogues of **1** wherein Mg is replaced by Mn, Ni and Cu. We successfully isolated the Mn and Cu analogues but could not form the Ni phase.

Figure 5A compares the CO_2 adsorption isotherms at 273 K of the $Mg(4\text{-}PyC)_2$ and its Mn, and Cu analogues. Since the order of the hardness of the metals is Mg >Mn> Cu, we would expect the M-N bond to go from weakest to strongest as Mg, Mn, Cu. Therefore, we would expect the gate opening to be more hindered as the M-N bond becomes stronger. With Mg, which should have the weakest M-N bond, we observe two gate-opening events, the first one occurring at ~0.15 bar. With Mn, we observe only one gate opening event and it occurs at higher pressure (~0.23 bar) than with the Mg analogue. This is consistent with the HSAB hypothesis. With Cu, we see no gating and presumably, the gates are locked in the open position whereas with Mg simulations suggested that the gates freely open and close without any gases, which closes off the channels.

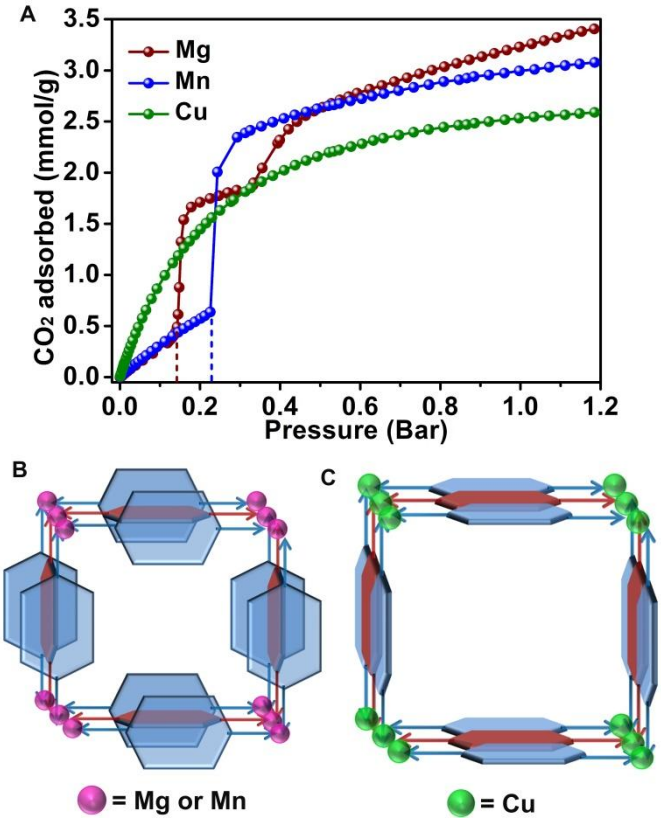

Figure 5. (A) Comparative CO_2 isotherms at 273 K for the Mg, Mn and Cu analogues of **1**. Highlighted are the onsets of the gate-opening pressures that shift to higher values following the HSAB rule. A schematic representation of the initial configuration for the Mg & Mn analogues (closed) and the Cu analogue (open) have been presented in figures B and C.

The initial configuration (before the gate-opening) of the 4-PyC analogues have been schematically represented in Figure 5B and 5C. In figure 5A, the closed-form of the Mn or Mg phases show only an initial surface adsorption before the gate opening (Mg: 0.44 mmol/g @ 0.14 bar; Mn: 0.64 mmol/g @ 0.23 bar) and they represent one extreme, while the open-form of the Cu phase (Figure 5B) shows much higher uptake (Cu: 1.18 mmol/g @ 0.14 bar and 1.52 mmol/g @ 0.23 bar) at the similar pressures, thus representing the other extreme.

Conclusions

We have shown how a non-porous and rigid solid, $Mg(4\text{-}PyC)_2$, can be made into a dynamic porous solid with good CO_2 uptake and selectivity through 'coordination flexibility'. The CO_2-specific gate-opening, observed in **1** and **2** that does not also result in large structural changes of the framework is unprecedented. Additionally, due to the ultra-microporous nature of the materials, the effect of the gate moiety rotation is drastic – changing a non-porous material into a porous one. Compared to other breathing phenomenon our hard-soft acid base assisted coordination flexibility could be relatively easier to embed into a range of extended metal-organic structures to make them functioning or operating more selectively under milder triggering conditions. Other interesting classes of systems where this chemistry or even the exact choice of metal and ligand are adoptable would be the metallo-cyclodextrins,[60] crystalline cavitands,[61] metal-organic nanotubular assemblies,[62] MOFs with large discrete cages,[63] crystalline molecular flasks,[64] and polycatenanes/pseudorotaxanes.[65] Most of these systems possess massive nano-sized discrete cages accessible to guest solvent but are locked for gases. This approach could expand their limits by unlocking these cages into gas-selective 1 or 2 or 3-D nanochannels.

Conflicts of interest

There are no conflicts to declare.

Acknowledgements

We acknowledge IISER-Pune and the MHRD-FAST program and University of Ottawa for the necessary funding. SN thanks DST, SERB and IISER Pune for the fellowship. RM thanks IISER Pune for fellowship. DC Thanks DST-Inspire for financial support.

Notes and references

1 H. C. Zhou, J. R. Long and O. M. Yaghi, *Chem. Rev*., 2012, **112**, 673−674.
2 J. K. Ryan, D. J. Timmons, Q.-R. Fang, J.-R. Li, T. A. Makal, M. D. Young, D. Yuan, D. Zhao, W. Zhuang and H.-C. Zhou, *Coordination Chemistry Reviews,* 2009, **253**, 3042–3066.
3 F. A. A. Paz, J. Klinowski, S. M. F. Vilela, J. P. C. Tome´, J. A. S. Cavaleiro and J. Rocha, *Chem. Soc. Rev*., 2012, **41**, 1088–1110.
4 S. Henke, A. Schneemann, A. Wütscher and R. A. Fischer, *J. Am. Chem. Soc*., 2012, **134**, 9464−9474.
5 S. Kitagawa and K. Uemura, *Chem. Soc. Rev.,* 2005, **34**, 109–119.
6 G. Ferey and C. Serre, *Chem. Soc. Rev*., 2009, **38**, 1380−1399.
7 S. Horike, S. Shimomura and S. Kitagawa, *Nat. Chem*., 2009, **1**, 695−704.
8 H. Sato, W. Kosaka, R. Matsuda, A. Hori, Y. Hijikata, R. V. Belosludov, S. Sakaki, M. Takata, and S. Kitagawa, *Science*, 2014, **343**, 167−170.
9 A. Schneemann, V. Bon, I. Schwedler, I. Senkovska, S. Kaskel and R. A. Fischer, *Chem. Soc. Rev*., 2014, **43**, 6062—6096.
10 L. Sarkisov, R. L. Martin, M. Haranczyk and B. Smit, *J. Am. Chem. Soc*., 2014, **136**, 2228−2230.
11 Z.-J. Lin, J. Lu¨, M. Hong and R. Cao, *Chem. Soc. Rev*., 2014 , **43**, 5867—5895.
12 R. K. Motkuri, P. K. Thallapally, H. V. R Annapureddy, L. X. Dang, R. Krishna, S. K. Nune, C. A. Fernandez, L. Liu and B. P. McGrail, *Chem. Commun*., 2015, **51**, 8421.
13 S. Yang, X. Lin, W. Lewis, M. Suyetin, E. Bichoutskaia, J. E. Parker, C. C. Tang, D. R. Allan, P. J. Rizkallah, P. Hubberstey, N. R. Champness, K. M. Thomas, A. J. Blake and M. Schröder, *Nat. Mater*., 2012, **11**, 710-716.
14 J. A. Mason, J. Oktawiec, M. K. Taylor, M. R. Hudson, J. Rodriguez, J. E. Bachman, M. I. Gonzalez, A. Cervellino, A. Guagliardi, C. M. Brown, P. L. Llewellyn, N. Masciocchi and J. R. Long, *Nature*, 2015, **527**, 357–361.
15 T. K. Maji, R. Matsuda and S. Kitagawa, *Nat. Mater*., 2007, **6**, 142.

16 K. Fukuhara, S.-I. Noro, K. Sugimoto, T. kutagawa, K. Kubo and T. Nakamura, *Inorg. Chem*., 2013, **52**, 4229−4237.
17 A. Schneemann, P.V ervoorts, I. Hante, M. Tu, S. Wannapaiboon, C. Sternemann, M. Paulus, D. C. F. Wieland, S. Henke and R. A. Fischer, *Chem. Mater*., 2018, **30**, 1667−1676.
18 S.-M. Hyun, J. H. Lee, G. Y. Jung, Y. K. Kim, T. K. Kim, S. Jeoung, S. K. Kwak, D. Moon and H. R. Moon, *Inorg. Chem*., 2016, **55**, 1920−1925.
19 P. K. Thallapally, J. Tian, M. Radhakishan, C. A. Fernandez, S. J. Dalgarno, P. B. McGrail, J. E. Warren and J. L. Atwood, *J. Am. Chem. Soc.*, 2008, **130**, 16842–16843.
20 A. J. Fletcher, K. M. Thomas and M. J. Rosseinsky, J. *Solid State Chem*., 2005, **178**, 2491–2510.
21 Z. Chang, D.-H. Yang, J. Xu, T.-L. Hu and Z.-H. Bu, *Adv. Mater.,* 2015, **27**, 5432–5441.
22 L. Li, R.-B. Lin, R. Krishna, X. Wang, B. Li, H. Wu, J. Li, W. Zhou and B. Chen, *J. Am. Chem. Soc.,* 2017, **139**, 7733–7736.
23 R. V. Belosludov, S. Sakaki, M. Takata, S. Kitagawa, P. A. P. Mendes, P. Horcajada, S. Rives, H. Ren, A. E. Rodrigues, T. Devic, E. Magnier, P. Trens, H. Jobic, J. Ollivier, G. Maurin, C. Serre and J. A. C. Sil, *Adv. Funct. Mater*., 2014, **24**, 7666–7673.
24 W. Yang, A. J. Davies, X. Lin, M. Suyetin, R. Matsuda, A. J. Blake, C. Wilson, W. Lewis, J. E. Parker, C. C. Tang, M. W. George, P. Hubberstey, S. Kitagawa, H. Sakamoto, E. Bichoutskaia, N. R. Champness, S. Yang and M. Schroder, *Chem. Sci*., 2012, **3**, 2993.
25 S. Bourrelly, P. L. Llewellyn, C. Serre, F. Millange, T. Loiseau and G. Ferey, *J. Am. Chem. Soc*., 2005, **127**, 13519-13521.
26 E. J. Carrington, C. A. McAnally, A. J. Fletcher, S. P. Thompson, M. Warren and L. Brammer, *Nat. Chem*., 2017, **9**, 882–889.
27 S. Shimomura, M. Higuchi, R. Matsuda, K. Yoneda, Y. Hijikata, Y. Kubota, Y. Mita, J. Kim, M. Takata and S. Kitagawa, *Nat. Chem*., 2010, **2**, 633–637.
28 B. Li, H.-M. Wen, W. Zhou and B. Chen, *J. Phys. Chem. Lett.,* 2014, **5**, 3468−3479.
29 Q.-Y. Yang, P. Lama, S. Sen, M. Lusi, K.-J. Chen, W.-Y. Gao, M. Shivanna, T. Pham, N. Hosono, S. Kusaka, J. J. Perry IV, S. Ma, B. Space, L. J. Barbour, S. Kitagawa and M. J. Zaworotko, *Angew. Chem. Int. Ed*., 2018, **57**, 1 – 7.
30 N. Klein, C. Herzog, M. Sabo, I. Senkovska, J. Getzschmann, S. Paasch, M. R. Lohe, E. Brunner and S. Kaskel, *Phys. Chem. Chem. Phys*., 2010, **12**, 11778–11784.
31 Q. Chen, Z. Chang, W.-C. Song, H. Song, H.-B. Song, T.-L. Hu and X. H. Bu, *Angew. Chem. Int. Ed*., 2013, **52**, 11550 –11553.
32 P. Horcajada, R. Gref, T. Baati, P. K. Allan, G. Maurin, P. Couvreur, G. Ferey, R. E. Morris and C. Serre, *Chem. Rev*., 2012, **112**, 1232–1268.
33 A. C. McKinlay, J. F. Eubank, S. Wuttke, B. Xiao, P. S. Wheatley, P. Bazin, J.-C. Lavalley, M. Daturi, A. Vimont, G. D. Weireld, P. Horcajada, C. Serre and R. E. Morris, *Chem. Mater*., 2013, **25**, 1592−1599.
34 P. Horcajada, C. Serre, G. Maurin, N. A. Ramsahye, F. Balas, M. Vallet-Regí, M. Sebban, F. Taulelle and G. Férey, *J. Am. Chem. Soc*., 2008, **130**, 6774–6780.
35 J. Seo, R. Matsuda, H. Sakamoto, C. Bonneau and S. Kitagawa, *J. Am. Chem. Soc*., 2009, **131**, 12792–12800.
36 C. Serre, F. Millange, C. Thouvenot, M. Nogues, G. Marsolier, D. Louer and G. Ferey, *J. Am. Chem. Soc*., 2002, **124**, 13519-13526.
37 C. Serre, S. Bourrelly, A. Vimont, N. A. Ramsahye, G. Mau-rin, P. L. Llewellyn, M. Daturi, Y. Filinchuk, O. Leynaud, P. Barnes and G. Férey, *Adv. Mater*., 2007, **19**, 2246–2251.
38 K. Sumida, D. L. Rogow, J. A. Mason, T. M. McDonald, E. D. Bloch, Z. R. Herm, T.-H. Bae and J. R. Long, *Chem. Rev*., 2012, **112**, 724–781.
39 M. Eddaoudi, H. Li and O. M. Yaghi, *J. Am. Chem. Soc*., 2000, **122**, 1391-1397.
40 H. Furukawa, N. Ko, Y. B. Go, N. Aratani, S. B. Choi, E. Choi, A. O. Yazaydin, R. Q. Snurr, M. O'Keeffe, J. Kim and O. M. Yaghi, *Science*, 2010, **329**, 424-428.
41 A. R. Millward and O. M. Yaghi, *J. Am. Chem. Soc*., 2005, **127**, 17998.
42 Q. Yang, S. Vaesen, F. Ragon, A. D. Wiersum, D. Wu, A. Lago, T. Devic, C. Martineau, F. Taulelle, P. L. Llewellyn, H. Jobic, C. Zhong, C. Serre, G. D. Weireld and G. A. Maurin, *Angew. Chem. Int. Ed.*, 2013, **52**, 10316 –10320.
43 G. E. Cmarik, M. Kim, S. M. Cohen and K. S. Walton, *Langmuir*, 2012, **28**, 15606−15613.
44 C. Serre, C. Mellot-Draznieks, S. Surblé, N. Audebrand, Y. Filinchuk and G. Férey, *Science*, 2007, **315**, 1828.
45 N. Nijem, H. Wu, P. Canepa, A. Marti, K. J. Balkus, T. Thonhauser, J. Li and Y. J. Chabal, *J. Am. Chem. Soc*., 2012, **134**, 15201−15204.
46 C. Mellot-Draznieks, C. Serre, S. Surble, N. Audebrand and G. Ferey, *J. Am. Chem. Soc*., 2005, **127**, 16273-16278.
47 J. Seo, C. Bonneau, R. Matsuda, M. Takata and S. Kitagawa, *J. Am. Chem. Soc*., 2011, **133**, 9005–9013.
48 D. Banerjee, H. Wang, A. M. Plonka, T. J. Emge, J. B. Parise and J. Li, *Chem. Eur. J*., 2016, **22**, 11816 – 11825.
49 A. Arami-Niya, G. Birkett, Z. Zhu and T. E. Rufford, *J. Mater. Chem. A*, 2017, **5**, 21389–21399.
50 P. Zhao, H. Fang, S. Mukhopadhyay, A. Li, S. Rudić, I. J. McPherson, C. C. Tang, D. Fairen-Jimenez, S. C. E. Tsang and S. A.T. Redfern, *Nat. Commun*., 2019, **10**, 999-1006.
51 M. Tu, C. Wiktor, C. Ro¨sler and R. A. Fischer, *Chem. Commun*., 2014, **50**, 13258—13260.
52 J. P. S. Mowat, V. R. Seymour, J. M. Griffin, S. P. Thompson, A. M. Z. Slawin, D. Fairen-Jimenez, T. Düren, S. E. Ashbrooka and P. A. Wright, *Dalton Trans*., 2012, **41**, 3937–3941.
53 J. Xiao, Y. Wu, M. Li, B.-Y. Liu, X.-C. Huang and D. Li, *Chem. Eur. J*., 2013, **19**, 1891–1895.
54 F.-X. Coudert, C. Mellot-Draznieks, A. H. Fuchs and A. Boutin, *J. Am. Chem. Soc*., 2009, **131**, 11329–11331.
55 R. Vaidhyanathan, S. S. Iremonger, G. K. H. Shimizu, P. G. Boyd, S. Alavi and T. K. Woo, *Science*, 2010, **330**, 650-653.
56 D. Saha, Z. Bao, F. Jia and S. Deng, *Environ. Sci. Technol.*, 2010, **44**, 1820.
57 Z. Zhao, Z. Li and Y. S. Lin, *Ind. Eng. Chem. Res*., 2009, **48**, 10015-10020.
58 A. C. Kizzie, A. G. Wong-Foy and A. J. Matzger, *Langmuir*, 2011, **27**, 6368-6373.
59 S. Nandi, S. Collins, D. Chakraborty, D. Banerjee, P. K. Thallapally, T. K. Woo and R. Vaidhyanathan, *J. Am. Chem. Soc*., 2017, **139**, 1734–1737.
60 K. J. Hartlieb, J. M. Holcroft, P. Z. Moghadam, N. A. Vermeulen, M. M. Algaradah, M. S. Nassar, Y. Y. Botros, R. Q. Snurr and J. F. Stoddart, *J. Am. Chem. Soc*., 2016, **138**, 2292−2301.
61 J. R. Holst, A. Trewin and A. I. Cooper, *Nat. Chem*., 2010, **2**, 915.
62 K. Otsubo, Y. Wakabayashi, J. Ohara, S. Yamamoto, H. Matsuzaki, H. Okamoto, K. Nitta, T. Uruga and H. Kitagawa, *Nat. Mater*., 2011, **10**, 291.
63 R. Vaidhyanathan, C. A. Bridges, D. Bradshaw and M. J. Rosseinsky, *Cryst. Growth Des*., 2010, **10**, 4348.
64 Y. Inokuma, M. Kawano and M. Fujita, *Nat. Chem*., 2011, **3**, 349.
65 L. Jiang, P. Ju, X.-R. Meng, X.-L. Kuang and T.-B. Lu, *Sci. Rep*., 2012, **2**, 668.